Modified Hairy Nanocrystalline Cellulose as Photobactericidal Nanofillers for Food Packaging Application

Roya Koshani[†,‡,§,₸], Jingbin Zhang[†], Theo G.M. van de Ven[‡,§,₸*], Xiaonan Lu[†], Yixiang Wang[†*]

[†]Department of Food Science and Agricultural Chemistry, McGill University, 21111 Lakeshore, Ste Anne de Bellevue, QC H9X 3V9, Canada

[‡]Department of Chemistry, McGill University, 801 Sherbrooke Street West, Montreal, QC, H3A 0B8, Canada

[§]Pulp and Paper Research Centre, McGill University, 3420 University Street, Montreal, QC, H3A 2A7, Canada

[₸]Quebec Centre for Advanced Materials (QCAM), 3420 University Street, Montreal, QC, H3A 2A7, Canada

*Corresponding authors:

theo.vandeven@mcgill.ca

yixiang.wang@mcgill.ca

Other authors email:

roya.koshani@mcgill.ca

jingbin.zhang@mail.mcgill.ca

xiaonan.lu@mcgill.ca

ABSTRACT

A photobactericidal hairy nanocrystalline cellulose was developed as a bio-inspired nanofiller for engineering self-disinfecting food packaging. A new version of hairy nanocellulose (HNC) functionalized with a high density of primary amine groups called ANCC was synthesized. As a natural photosensitizer, rose bengal (RB) was then covalently linked to ANCC via an aqueous-based bioconjugation reaction, as confirmed by ^{13}C nuclear magnetic resonance (NMR) and Fourier transform infrared (FTIR) spectroscopies. Antibacterial effect of RB-ANCC conjugate was evaluated against two major foodborne pathogens, namely *Listeria monocytogenes* and *Salmonella enterica* serotype Typhimurium. RB-ANCC conjugate inactivated over 80% of both pathogens upon normal light irradiation. A remarkable photo-inactivation of *S.* Typhimurium was achieved using RB-ANCC in which cases free RB had no effect. We then selected two materials (*i.e.*, a cellulose-based film and a web of electrospun nanofibers) to incorporate RB-ANCC for further evaluating antimicrobial activity, and identified that the activity was due to a combination of photodynamically generated reactive oxygen species by RB and an electrostatically-induced cell wall disruption by cationic ANCC. The developed RB-ANCC conjugate processed via green chemistry is regarded as a promising photobactericidal nanofiller and can be potentially used for food packaging.

KEYWORDS: aminated hairy nanocrystalline cellulose, rose bengal, DMTMM coupling, photobactericidal, electrospun nanofibers, cellulosic films

INTRODUCTION

Due to a soaring population growth, reliable access to safe food has turned into a global challenge. According to the statistics of world health organization (WHO)-reported foodborne diseases, almost 1 in 10 people fall ill and 33 millions of healthy life years are lost each year.[1] One of the most effective strategies for controlling foodborne pathogens is developing antimicrobial materials/surfaces that are in a direct or an indirect contact with foods. Conventional ways integrate antibacterial reagents such as antibiotics, fungicides, antiviral drugs, etc., onto polymeric matrices. However, extensive use of these antibacterial substances has become a great threat to human health due to the emergence of antimicrobial-resistant bacteria.[2]

Photodynamic therapy (PDT) is proposed as a promising alternative to the conventional antimicrobial agents to eliminate/reduce bacteria. This technique requires the interaction of three non-toxic agents including oxygen, light and a photoactive molecule, which is referred as photosensitizer. In the presence of the light, photosensitizers are excited by adsorbing energy and then interact with oxygen, resulting in the generation of reactive oxygen species (ROS). The reactive singlet oxygen together with free radicals can readily damage the integrity of bacterial cells.[3, 4] Since inactivating microorganisms by cytotoxic ROS is based on irreversible non-specific damage of the vital structural biomolecules, such as DNA, proteins, and lipids, it is believed that photodynamic therapy would not easily generate antimicrobial resistance.[5, 6] To endow surfaces with photobactericidal property, a facile and efficient way is to develop photoactive nanofillers and incorporate them into polymeric matrices. As easily manipulatable components, nanofillers are used to improve the physicochemical properties of composites and films.[7]

As the photosensitizer, natural photodynamic RB is promising in this context due to its biocompatibility, relatively low cost, and low toxicity. RB possesses less antibacterial efficacy on

Gram-negative bacteria than on Gram-positive ones. Gram-negative bacteria have an outer lipopolysaccharidic cell membrane that causes an additional penetration barrier to many compounds. One of the common strategies to overcome the initial obstacle in photodynamic inactivation of Gram-negative bacteria is linking photosensitizers with cationic compounds.[8, 9] However, most cationic membrane-disrupting agents such as cationic surfactants[10], poly-lysines[11] and quaternary ammonium compounds[12] are toxic, expensive, and non-biocompatible.

With consideration to all the above-mentioned issues, we focused our engineering pathway to design a cationic photobactericidal nanofiller derived from bio-based HNC and RB. A systematic approach was taken to develop and characterize the materials. In the first step, a novel form of HNC functionalized with a high content of primary amine groups, referred to as ANCC, was developed. HNCs, in addition to crystalline segments that are also present in conventional nanocrystalline celluloses (NCCs), contain amorphous chains protruding from the two ends.[13] ANCC was exploited for attaching carboxyl-bearing RB onto it through bioconjugation reaction. Our hypotheses are that (i) the positively charged conjugate facilitates anchoring photoactive RB to the cell membrane/wall or can penetrate the cells via electrostatic interaction and (ii) ANCC, similar to chitosan, can itself have antibacterial activity, along with RB, inducing a synergistic antibacterial effect. Increasing the solubility, facilitating entering of the photosensitizer into cells, and preventing the easy release of RB in the food environment can be other features of a RB-ANCC conjugate. Notable also is that since the singlet oxygen and hydroxyl radicals have a short lifetime, the localization of RB largely determines its photoinactivation efficiency. In a next step, we selected two different types of cellulosic materials to develop photo-bactericidal materials: anionic carboxyl modified cellulose (CMF) films, coated by RB-ANCC, and webs of electrospun cellulose acetate (CA) nanofibers in which RB-ANCC was incorporated. After fully

characterization of the newly developed ANCC, the successful attachment of RB through a facile aqueous-based 4-(4,6-dimethoxy-1,3,5-triazin-2-yl)-4-methylmorpholinium chloride (DMTMM) coupling chemistry was confirmed by FTIR and ^{13}C NMR spectroscopy. Antimicrobial assays of nanomaterials and surfaces were undertaken to evaluate their activity against Gram-positive *Listeria monocytogenes* and Gram-negative *Salmonella enterica* serotype Typhimurium, common pathogens found in food.

EXPERIMENTAL SECTION

Q90 bleached softwood kraft sheet was provided by FPInnovations (Pointe-Claire QC Canada) and milled as starting cellulose material. Cellulose acetate from cigarette filters was kindly provided by Celanese Corporation (Irving, US). All the chemicals, described in Supporting Information, were reagent-grade and were used as received.

The light source utilized in this study was two 13-W daylight compact fluorescent lamps. This type of the lamps has the same color properties and spectral power distribution as the regular fluorescent luminaires used at the food-supplying factories, hospitals, stores, and restaurants.

Material Synthesis

Hairy Aminated Nanocrystalline Cellulose (ANCC)

ANCC was synthesized via the oxidation of C_2–C_3 hydroxyl groups in the cellulose glucose chains followed by the reduction of the resulting aldehyde groups to primary amine groups. A visual demonstration of the procedure is found in Scheme 1 and Figure 1a. For this purpose, softwood pulp powder (10 g) was added to a solution of $NaIO_4$ (13.2 g) and NaCl (38.7 g) in DI water (625 mL) prepared at an aluminum foil-covered beaker. The pulp was stirred at room temperature for 42 h, and then 10 mL of ethylene glycol was added to this mixture to stop the reaction by quenching the residual periodate. The resulting dialdehyde modified cellulose (DAMC) fibers was washed

by vacuum filtration and thoroughly dried at room temperature. A small amount of DAMC was taken at this step and was used to determine the aldehyde content (see the protocol's details in Supporting Information).

In the next step, fully-dried DAMC (4 g), $NH_4CH_3CO_2$ (3.28 g), and NH_3 (6 mL) were dispersed in anhydrous ethanol (200 mL), and the slurry was stirred at 80 °C under reflux condition for 18 hrs. Then, the temperature was reduced to room temperature and 0.54 g of $NaBH_4$ was gradually added followed by stirring for an additional 1 hr. The brownish diamino cellulose (DamC) fibers were rinsed with DI water. DamC (2 g) was redispersed in DI water (200 mL), the pH was adjusted to ~2.5 by HCl addition and the mixture was stirred for 1 hr so that the fibers were well solubilized. Afterward, the suspension was stirred at 60 °C in an oil bath for 2 h and subsequently centrifuged to remove the non-fibrillated fibers (~40%). The supernatant containing ANCC was precipitated by adding isopropanol (the weight of propanol is 1.5 times of supernatant), collected by centrifugation at 5000 rpm for 15 min, and stored for further usage.

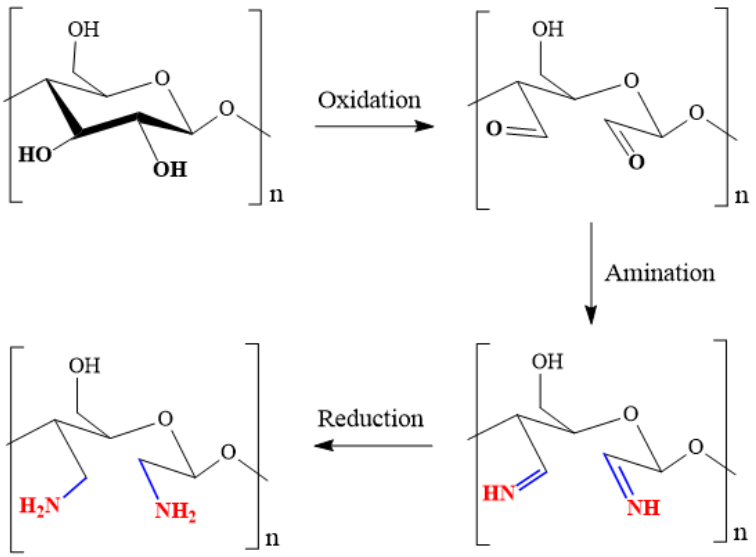

Scheme 1. Periodate oxidation of cellulose fibers to produce dialdehyde modified cellulose (DAMC) followed by reductive amination of dialdehyde groups, occurring in two successive steps. The first part

is the nucleophilic addition of the carbonyl group of the aldehyde groups using ammonia to form an imine. The second part is the reduction of the imine to an amine using $NaBH_4$ as reducing agent.

RB-ANCC Conjugate

To attach RB molecules onto the hairs of the ANCC, the carboxylic group of the RB can be reacted with the amine groups of the ANCC through a bioconjugation reaction. For this purpose, the carboxyl groups need to be activated via reaction with DMTMM and formation of an active ester intermediate (see Scheme 2). The amount of activator was calculated based on the carboxylic content of RB. The RB suspension (50 mL of 0.2% wt.; ~ 0.098 mmol of carboxyl groups) and DMTMM (0.1 M solution) at a 1:1 mol ratio of activator to carboxyl groups were reacted for 60 min at 37 °C. The amount of DMTMM was considered with 15% excess. It should be noted that since the carboxyl groups of RB are in the sodium form, no pH changes occur when being dissolved in DI water. Then, ANCC was added to the activated RB at a 1:0.5 weight ratio (~50 mg), equal to the 1:0.5 mol ratio of amine groups: carboxyl groups. The pH of the suspension remained unchanged at ~ 6.5 and the reaction proceeded at 37 °C for an extra 60 min. Excess DMTMM, unreacted RB molecules and byproducts were removed by purification using dialysis bags. The concentration of the grafted RB was estimated using ultraviolet−visible (UV-Vis) spectrophotometry (Cary 5000 UV−vis−NIR spectrophotometer, Agilent Technologies, Santa Clara, CA, U.S.A.) because RB shows a distinct absorption peak at λ_{max} of 550 nm. A calibration curve was plotted as a function of different RB concentrations (see Figure S1).

Photodynamically Active Cellulosic Materials

CMF Film

To make films of CMF, a previously reported protocol by Moradian et al. was followed.[14] Briefly, CMF with carboxyl density of ~1 mmol g^{-1} (2 g) were dissolved in DI water (50 mL) and, after

adding NaOH (2 g) and mixing, dopes were made, then degassed by centrifugation at 1000 rpm for 5 min. Afterwards, the solution was casted in rectangular molds and immersed in a sulfuric acid bath (10 wt. %). Cellulose dope was regenerated entirely, forming an insoluble cellulose film in 6 min. The films were washed with tap water several times to make sure all the chemicals were washed out. Wet films were put on a glass plate for a few hours to be air-dried.

To incorporate the 2.5 wt. % RB-ANCC onto the films, a 3×6 cm^2 piece (~ 1 g) was immersed in RB-ANCC suspension (5 mL of 5 mg mL^{-1}) and left in drawer overnight for maximum electrostatic adsorption and drying the films (see Figure S3 a). The amount of 2.5 wt. % RB-ANCC was chosen since it proved the best deposition condition for CMF films.

Electrospun Nanofibers

For this purpose, grinded CA (1.2 g) and RB-grafted ANCC (~30 mg) were dissolved in pure acetic acid (12 mL of 85 wt. %) and stirred at room temperature for 24 hrs. Nanofibrous webs containing 2.5 wt. % RB-grafted ANCC were fabricated by an electrospinning apparatus (Tong Li Tech, Shenzhen, China) at room temperature. Nanofibers were peeled off after immersing 3×6 cm^2 pieces in DI water (250 mL) for 2 min (see Figure S3 b).

Material Characterization

Determining the Amine Content

To measure the amount of amine functional groups on the surface of ANCC, conductometric titration was carried out using an 836 Titrando titrator (Metrohm, Switzerland). For this purpose, the sample (35 mg) was dispersed in Milli-Q water (100 mL). The pH was adjusted to 11.5 by adding 0.1 M NaOH solution. Then, 10 mM HCl at a rate of 0.1 mL min^{-1} was added to the suspension and the conductivity was measured until the pH reached ~3.6. That part of the

conductivity-vs-volume curve characterized by a negligible change in the conductivity represents a weak base and can be used to calculate the amine content in mmol per gram of ANCC.

AFM, TEM and SEM Imaging

The morphology of ANCC and cellulosic surfaces were analyzed by multimode atomic force microscopy (AFM) (Digital Instruments/Veeco, Santa Barbara, CA, U.S.A.) and scanning electron microscopy (SEM) (Zeiss 1540XB, Germany). The sizes of ANCC particles were determined using transmittance electron microscopy (TEM) imaging with an FEI Tecnai 12 Biotwin operating at 120 kV. The details of preparing specimens and imaging are described in Supporting Information.

ζ-Potential and Hydrodynamic Size of ANCC

To examine the charge status of the amine groups at pHs of 3.5 and 5, the ζ-potential of ANCC (0.1 wt.%) was measured through electrophoretic mobility using zetasizer Nano ZS (Malvern Instruments, U.K.).

The hydrodynamic size of the ANCC (0.1 wt. % suspension) was measured using a Brookhaven light scattering instrument BI9000 AT digital correlator.

Fourier Transform Infrared (FTIR) Spectroscopy

ANCC, RB-ANCC, RB-ANCC-incorporated cellulosic film and nanofiber were characterized using FTIR spectroscopy (Spectrum Two, PerkinElmer, U.S.A.) with a single bounce diamond attenuated total reflectance (ATR) accessory was employed. Each spectrum was an average of from 32 scans at transmission mode from 400 to 4000 cm^{-1} with a resolution of 4 cm^{-1}.

^{13}C Cross-Polarization Magic Angle Spinning (CP-MAS) Nuclear Magnetic Resonance (NMR) Spectroscopy

Solid-state NMR was used to confirm the covalent linking of the RB molecules to the ANCC through bioconjugation reaction. ANCC, RB and RB-ANCC were characterized using a VNMRS-400 wide bore spectrometer operating at 399.9 MHz for ^{1}H and 100.5 MHz for ^{13}C in a 4 mm Varian Chemagnetics double-resonance probe. The recycle delay was 4 s. ANCC and RB-ANCC were spun at 8 kHz with a CP contact time of 2 ms and 5188 scans (6 hrs) were collected. For pure RB, to prevent the formation of lots of radicals during spinning, it was spun faster at 14 kHz and a total of 6336 scans (4.5 hrs) was collected.

Evaluation of Antibacterial Activity

Determining Antimicrobial Effect Using the Plating Assay

The conventional plating assay was performed to assess the antimicrobial efficacy of photodynamically active nanomaterials on *L. monocytogenes* and *S.* Typhimurium. Briefly, 1 mL of bacterial overnight culture was centrifuged at 15,000 ×*g* for 2 min, and the resultant cell pellets were resuspended in 1 mL of phosphate-buffered saline (PBS, pH =7.4). The preparation's details of overnight culture are available in Supporting Information.

Different concentrations of ANCC, RB, and RB-ANCC (2 mL) were mixed with TSB (1 mL) and bacteria suspension with a concentration of ~10^{9} CFU mL^{-1} (10 μL). The final RB concentrations of 0, 20, 40, 100, 210, and 425 ppm were subsequently tested. To obtain a homogeneous solution, the mixture was shaken (120 rpm) at 37 °C for 15 min in dark. Afterward, these samples were exposed to white light at a distance of ca. ~30 cm and an angle of 45° for 40 min, except ANCC samples were incubated in a rotation manner at 120 rpm for 3 hrs at 37 °C. The same series of RB and RB-ANCC samples were kept in dark as the control groups.

To test the antimicrobial effect of CMF films and CA nanofibers incorporated with RB-ANCC, these cellulosic materials at a dimension of 1 cm × 1 cm were fully immersed into a bacterial suspension (2 mL) with a concentration of ~10^6 CFU mL^{-1}, and they were exposed to white light in the same condition as aforementioned. The same series of samples were kept in dark as the control groups. The antimicrobial efficacy of CMF films and CA nanofibers without RB-ANCC conjugates (see Figure S3) were also tested to investigate the role of RB-ANCC in inhibiting pathogenic bacteria. After light treatment, 100 μL of each bacterial suspension was spread onto the surface of TSA in duplicate for viable bacterial cell enumeration. The antimicrobial effect of these materials was obtained by comparing the bacterial number of the control groups and light-treated groups.

Disk Diffusion Assay

The disk diffusion assay was performed to examine the diffusibility of ROS generated from photodynamically active surfaces. In brief, a bacterial suspension (100 μL, ~10^6 CFU mL^{-1}) was spread on TSA plates. CMF films and CA nanofibers were cut into small circles with a diameter of 1 cm and squares with a dimension of 1 cm × 1 cm and placed on the plates inoculated with bacteria. One set of the plates were irradiated for 40 min at a distance of 30 cm under the lamp, while another set of the plates were kept in dark as the control group. All plates were incubated at 37 °C for 24 hrs. Then, the zone of clearance on each plate was measured. Specifically, the diameter of the clear zone including the films was measured in three different directions, and the average was reported as the zone of inhibition.

RESULTS AND DISCUSSION

Morphological and Dimensional Analysis of ANCC

To examine the morphology and the size distribution of newly developed ANCC particles, AFM and TEM images were obtained and the results are shown in Figure 1b-d. ANCC is a rod-shaped particle with a length of ~120 nm and a diameter of ~5 nm. The morphology and the dimension of the aminated nanoparticles are the same as those of previous NCCs isolated via the oxidation reaction[13, 15] and acid hydrolysis[16]. The TEM-measured length of ANCC is also close to the value obtained from DLS measurements which is, on average, 140 nm. The DLS size of ANCC is in the size range of hairy electrosterically stabilized NCC, referred to as ENCC, in our previously reported studies.[13, 15] ENCC's size varies from 200 nm in DI water to 100 nm with increasing salt. Since the direct imaging techniques can only depict the crystalline body of HNCs, indirect proofs for the presence of amorphous cellulose chains protruding from their poles are presented in next section.

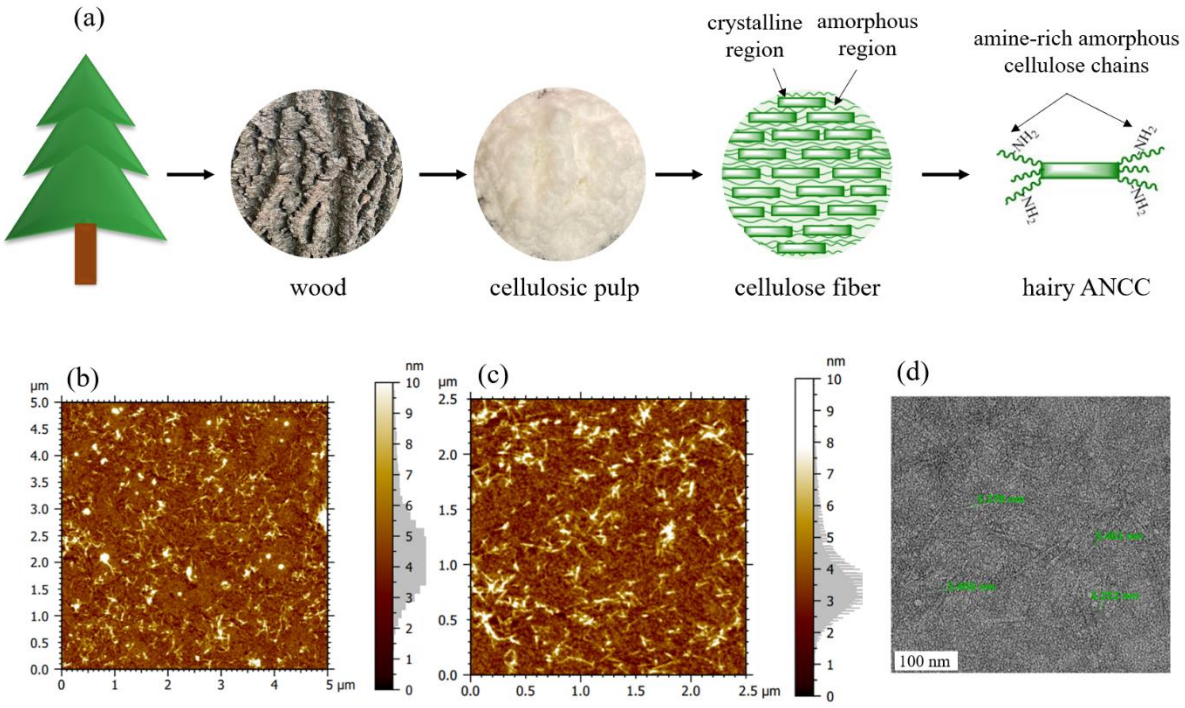

Figure 1. (a) Schematic diagram illustrating the general workflow for the isolation of hairy ANCC from cellulosic biomass via the two-step oxidation-reduction method; (b, c) AFM image of ANCC particles, showing the crystalline body of the nanowhiskers, similar to conventional NCCs at two scales of 5×5 μm and 2.5×2.5 μm; (d) TEM image indicating ANCC particles with the dimensions ~120 × 5nm.

Analyzing Surface Functional Groups of ANCC: Conductometric Titration and ζ- potential

The amine content of the ANCC was measured using conductometric titration by titrating the primary amine groups with a strong acid (HCl) which was found to be ~3.5 mmol per gram of ANCC (Figure 2). Since the amine content of ANCC exceeds the theoretical maximum surface charge content of a conventional NCC particles, this type is likely architecturally similar to previously reported ENCC particles.[15] In fact, ANCC particles have also protruding cellulose chains but with amine groups. The amorphous cellulose chains, known as hairs, are more accessible than the crystalline regions, which make HNC suitable for high-density functionalization. Complete conversion leads to the transformation of all three hydroxyl groups in the glucose units and thus an amine content of 18.5 mmol per gram or DS of 3. Here, degree of

substitution (DS) is defined as an average number of hydroxyl groups that are converted to amine groups. Therefore, the DS of the synthesized ANCC was 0.6.

Aldehyde contents of DAMC and ANCC were also measured. The initial aldehyde content of the DAMC oxidized by periodate was ~7.5 mmol g^{-1}, while amination reduced the content to ~4 mmol g^{-1}, implying ANCC has an amine content of ~3.5 mmol g^{-1}. The aldehyde content measurement implies a less than 50% amination reaction efficiency. This could be either due to the water remaining in air-dried DAMC fibers before the amination reaction or due to the closing of pores as a result of drying, thereby reducing the accessibility of all parts of fibers to the chemicals. The remaining water in fibers interferes in the reaction by hydrolyzing ammonia to ammonium and hydroxide. In cases that full conversion needs to be targeted, solvent exchange of fibers from water to ethanol is suggested as a solution for increasing the efficiency instead of drying.

The ζ-potential of ANCC was also determined which is, on average, +15 mV at pH = ~ 4.5 confirming the positive charges. The value reached at +30 mV by decreasing the pH ~ 3.5. Basically, at low pHs, the amine groups are highly protonated, thus creating positive charges, while at high pHs, they are deprotonated holding no charges or slightly negative charges. Therefore, in this work, besides taking advantage of the amine groups for covalent attachment of the carboxyl-bearing RB, the free amine groups can keep the surfaces positively charged. As the pH of most foods are in the acidic range or less than 7, they can be helpful in inducing positive charges on surfaces with deposited ANCC particles.

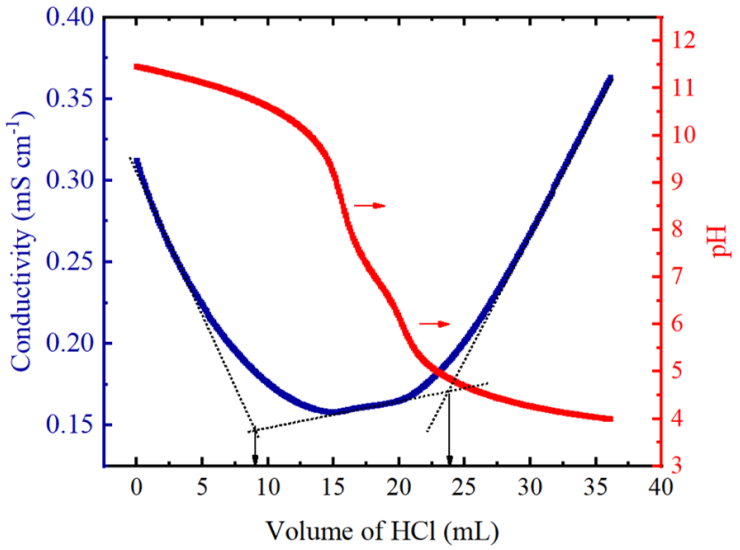

Figure 2. Conductometric titration of ANCC using a strong acid (HCl, 0.01 M), indicating that ~15 ± 1 mL of acid (shown with black arrows) is required to neutralize all the weak base, attesting to a functional group content of ~4 mmol of NH_2 per gram of ANCC with two pK_b's of 6 and 8.5 shown with red arrows.

Spectroscopic Analysis of RB-ANCC

As schematized below (Scheme 2), bioconjugation can occur between the primary amine groups of ANCC and the carboxyl groups of RB via DMTMM chemistry to create amid bonds. This strategy was previously used by our group for developing antibacterial lysozyme-NCC[16] and fluoresceinamine-NCC conjugates[17]. This method is facile, fast and requires no organic solvent. Here, we exploited only 2 mmol g^{-1} amine groups for covalently attaching the photoactive RB and left the rest of the amine groups unchanged. This is beneficial to achieve positively charged RB-ANCC conjugates to which the bacteria can rapidly and strongly attach (see Figure S5). Thus, the free radicals generated from bactericidal RB can function more effective in close contact with bacteria. This property also allows the amine groups to be accessible for further modifications *e.g.*, linking with other types of antibacterial agents or surface modifiers, which are desirable for surface

engineering. Obviously, there is room for optimization here to tailor the RB-ANCC conjugate based on the requirements of different types of photodynamic platforms.

Covalent bonding between the RB and ANCC was achieved by the reaction of the active ester on the surface of the activated RB with one amine group of the ANCC, leading to the formation of an amide group, accompanied by the release of a molecule of 4,6,-dimethoxy-1,3,5-triazine (DMT). The reaction mechanism for this bioconjugation reaction is illustrated in Scheme 2. ATR-FTIR and NMR spectroscopy were employed to confirm the amide bond formation in the resulting RB-ANCC.

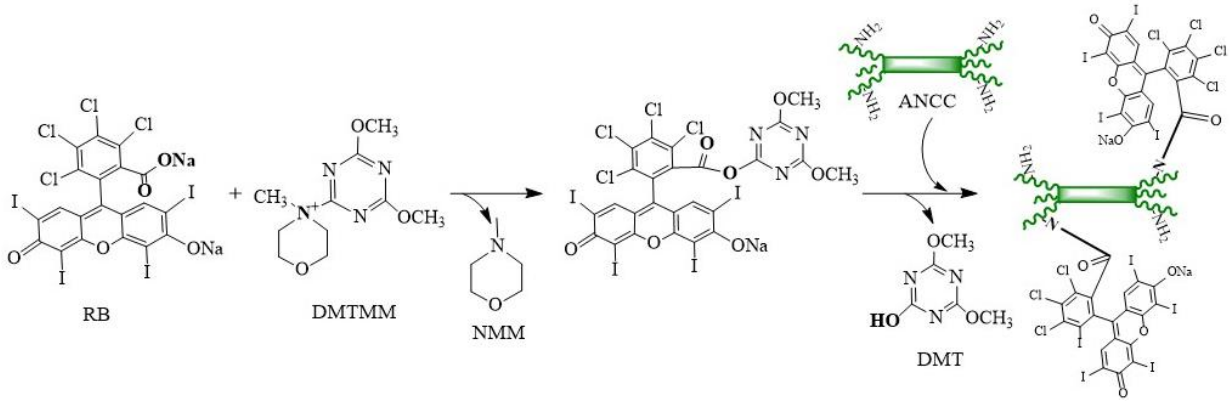

Scheme 2. Synthesis of photoactive RB-ANCC conjugates using DMTMM activator at 37 °C for 1 hr. The resulting ester on the surface of RB is attacked by one of the free amines on the surface of ANCC at neutral pH, yielding an amide, accompanied by the release of a molecule of DMT.

FTIR

FTIR spectra of ANCC, pure RB, RB-ANCC were collected which allows the qualitative analysis of the functional groups on the surface of these nanomaterials. The results are shown in Figure 3a. First, FTIR spectroscopy was used to prove the presence of amine groups located on the surface of ANCC. In the FTIR spectrum of ANCC, the absorption peaks of primary amine groups, basically appearing around 3400-3250 cm^{-1}, overlap with the stretching vibrations of O─H in its cellulosic structure. Thus, it cannot be clearly detected; instead, ANCC shows a broad sharp peak

298 at 1635 cm^{-1} for the C─NH_2 bending vibrations. Also, disappearance of the two characteristic
299 peaks of aldehyde groups at 1726 cm^{-1} and 878 cm^{-1} [18] implies the conversion of the aldehyde to
300 amine groups. To easily follow the changes in chemical compositions of the original cellulose,
301 DAMC and ANCC, FTIR spectra are provided in Figure S6. Therefore, the above analysis
302 confirms that ANCC was successfully synthesized.
303 In the case of pure RB, the C═O stretching vibrations of the carboxyl groups in the sodium form
304 are observed at 1610 cm^{-1}. The peaks at about 1534, 1488, and 1431 cm^{-1} are assigned to the
305 vibration of aromatic ring frame. In addition, the peaks at 1228 cm^{-1}, 1020 cm^{-1} and 758 cm^{-1} are
306 attributed to C–O–C groups, the Na–O bond and C–Cl stretching vibrations, respectively.[19]
307 FTIR spectrum of RB-ANCC was analyzed to confirm the successful covalent bonding between
308 functional groups of ANCC and RB. After the formation of RB-grafted ANCC through
309 bioconjugation reaction, the new peak at 1690 cm^{-1} could be associated with C═O stretching
310 vibrations as a result of the amide bond formation. The disappearance of the peak at 1610 cm^{-1} of
311 RB also implies the involvement of the carboxyl groups in the bioconjugation. Another new weak
312 peak appeared at 1580 cm^{-1} corresponds to unreacted NH_2 groups.[20] The peak which appeared at
313 1730 cm^{-1} is related to C═O stretching of the ketone groups in RB which did not appear at the
314 spectrum of pure RB due to overlap with the broad peak of the carboxylic acids.
315 The FTIR spectra of cellulosic films and nanofibers before and after incorporation with RB-ANCC
316 are shown in Figure 3b and 3c. For all samples, the peaks in the ranges around 3330 cm^{-1} and 2900
317 cm^{-1} are associated with the O–H and C–H stretching vibrations, respectively on the cellulose
318 structure. The characteristic peak at 1730 cm^{-1} for the CMF film represents C═O stretching of
319 carboxyl groups in the protonated form. For CMF film deposited with RB-ANCC (Figure 3b), the
320 peaks of the conjugate are clearly detectable. As RB-ANCC has extensively deposited onto the

surface of CMF film via electrostatic interaction, the conjugate's peaks appeared stronger than to the CMF's peaks. For nanofibers with incorporated RB-ANCC, the new sharp peak at 1580 cm^{-1} implies that the incorporation of RB-ANCC in the CA polymeric network was successful.

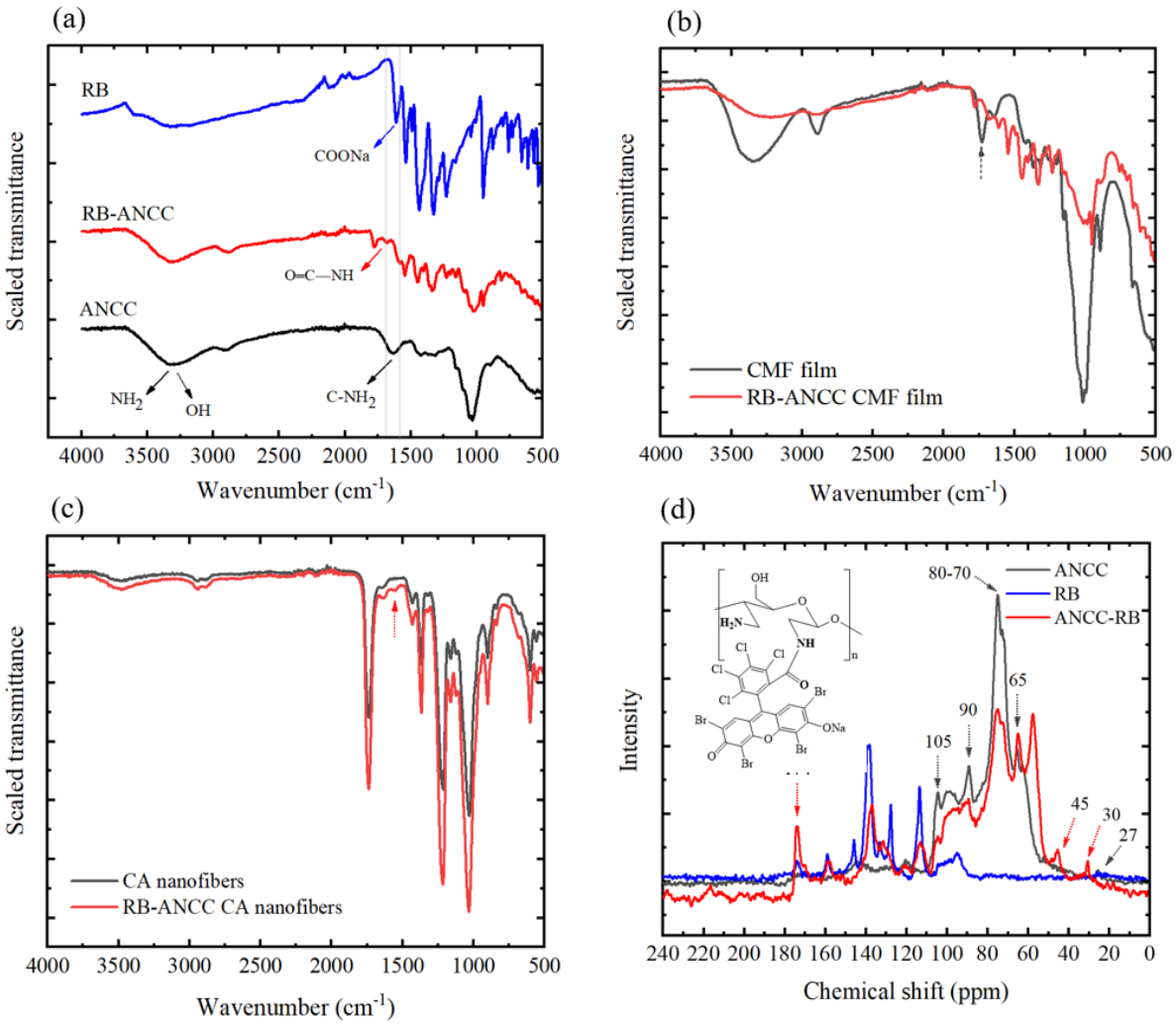

Figure 3. (a) FTIR spectra of ANCC, RB and RB-ANCC; (b) FTIR spectra of CMF film and CMF film with electrostatically deposited RB-ANCC; (c) FTIR spectra of CA nanofiber and CA nanofiber incorporated with RB-ANCC; and (d) solid-state ^{13}C CP/MAS NMR spectra of ANCC, pure RB, RB-ANCC.

Solid-State ^{13}C CP/MAS NMR

To further study the chemical properties of the ANCC, RB and RB-ANCC, solid ^{13}C NMR spectra were acquired. This also provides information about the formation of amide linking bonds in RB-

ANCC formed by DMTMM-mediated bioconjugation reaction. The results are displayed in Figure 3d.

In RB spectrum, the broad peak at 174 ppm corresponds to the carbonyl signals (C═O) of the carboxyl groups. The resonances appeared from 160 to 105 ppm are assigned to the aromatic carbons [21].

In the ANCC spectrum, the multiple peaks appearing at 105 to 55 ppm arise from the carbons of glucose units in its cellulosic structure specified as: 65 ppm for C6 of the primary alcohol group, 80-70 ppm for C2, C3, C5, 90 ppm for C4 and 105 ppm for anomeric C1.[22, 23] The narrow resonance at 90 ppm corresponds to C4 of anhydroglucose units in the crystalline parts. The sharp peak of C4 in ANCC spectrum itself implies the formation of the crystalline nanoparticles. In the pristine cellulose spectrum[22], a broad peak typically appears at 85 ppm which is the characteristic of C4' of the anhydroglucose units in the amorphous parts. The C4' peak is not detectable for ANCC; thus, the claim that shortening of hairs occurs as a result of acid hydrolysis is strengthened. The peak appearing at ~27 ppm could be associated with the carbons of primary amine groups (C—NH_2) introduced on the C2 and C3.

In the RB-ANCC spectrum, the sharp peak at 174 ppm corresponds to the carbonyl signals of the amide linking bonds (O═C—NH) formed between carboxyl groups of RB and primary amine groups of ANCC.[24] The peaks of carbons in ANCC cellulosic structure and aromatic rings in RB structure are clearly observed between 105 to 55 ppm and 160 to 105 ppm, respectively. The peaks at 45 ppm and 30 ppm can be attributed to the carbons of free primary amines, undergoing a shift compared to the amine peak of ANCC. This is a strong proof for the presence of primary amine groups in both linked and free form in RB-ANCC conjugates. Along with FTIR and NMR analysis,

the absorption behavior of ANCC and RB before and after covalent linkage was examined using UV-vis spectroscopy (see Figure S2).

Morphological Analysis of Materials Incorporated with RB-ANCC

The incorporation of RB-ANCC conjugate into CMF film and electrospun nanofibrous materials was investigated by AFM and shown in Figure 4. By studying these images, rod-like ANCC particles are observable on both films, although the resolution is less than that of isolated nanoparticles (Figure 1). RB-grafted ANCC particles were well dispersed and fixed in the film (Figure 4a) and nanofibrous web (Figure 4b). It can minimize the risk of photosensitizer diffusion and contamination of food products, which are in direct contact with packages. At the same time, photobactericidal ANCC particles can be activated by light to generate ROS to oxidatively kill bacteria, thereby keeping the surfaces decontaminated. The CA nanofibrous webs were also examined by SEM imaging (see Figure S4), which did not show any obvious morphological difference between the nanofibers with and without RB-ANCC incorporation. All nanofibers exhibited a smooth surface, but the diameter of nanofibers with RB-ANCC (184 ±76 nm) was larger than those with no RB-ANCC (56 ± 18 nm). Similar phenomenon was also observed when surface-modified cellulose nanowhiskers were added in electrospun prolamin protein fibers.[25]

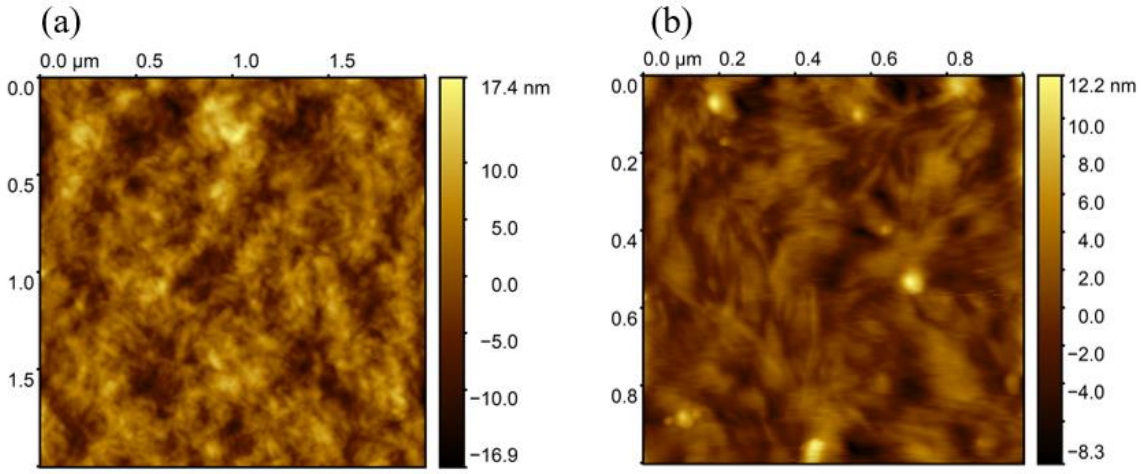

Figure 4. AFM height images of (a) CMF film with deposited RB-ANCC and (b) electrospun CA nanofiber with incorporated RB-ANCC.

Antibacterial Tests

In this study, the antimicrobial effects of RB and ANCC in free and grafted forms, as well as CMF films and CA nanofibers on *L. monocytogenes* and *S.* Typhimurium were tested. Gram-positive *L. monocytogenes* was selected because this pathogenic bacterium is commonly detected in foods stored at refrigerated temperature.[26] *S.* Typhimurium was chosen because this Gram-negative pathogen commonly spreads via the fecal-oral route through contaminated food and water sources.[27] Photobactericidal RB compound was conjugated to ANCC, and the potential of this conjugate in developing antibacterial photodynamically active nanofillers was evaluated. The bactericidal activity of nanomaterials and the corresponding surfaces was analyzed by using the plating assay and disk diffusion method.

Bacterial Viability: ANCC, RB and RB-ANCC

ANCC. ANCC carrying a high local density of amine groups could be a good cationic candidate for generating antibacterial activity. We hypothesized that ANCC could exhibit similar antimicrobial activity to other cationic antimicrobials, which inhibit bacterial growth by

electrostatically attaching to the negatively charged bacterial cell membrane. To confirm our hypothesis, we tested the viability of *L. monocytogenes* and *S.* Typhimurium after exposure to ANCC for 3 hrs. The reduction in bacterial cell count is shown in Figure 5a.

ANCC at concentrations of 1000 ppm and 700 ppm started inactivating *L. monocytogenes* and *S.* Typhimurium, respectively. At the concentration of 1500 ppm, ANCC reduced the number of viable bacteria to ~20% for *L. monocytogenes* and ~50% for *S.* Typhimurium. The antibacterial efficiency of ANCC could be further improved by optimizing the amine contents. In the acidic environment, protonation of amine groups occurs so as to increase the positive charges, resulting in the enhanced antibacterial efficiency of ANCC. Similar to other cationic antimicrobials (*e.g.*, chitosan[28], ε-poly-L-lysine[11] and quaternary ammonium compounds[29]), the mechanism of action of ANCC is likely through the adsorption onto the negatively charged cell surface and damaging the outer membrane to increase cell wall permeability and reduce adenosine triphosphate (ATP) biosynthesis. ATP is responsible for energy transport within the cell and essential for many bacterial processes.[30] Previous studies demonstrated that amine-functionalized nanocrystals could permeate cell membrane while carboxyl-functionalized homologues did not cause membrane disruption of non-phagocytic cells.[17, 31] However, carboxyl-bearing hairy ENCC was shown to enter cells by phagocytosis[17], which can also occur for ANCC. As shown in Figure 5a, the antibacterial effect of ANCC was more significant against Gram-negative *S.* Typhimurium than Gram-positive *L. monocytogenes* probably because of the thicker and more rigid cell wall of Gram-positive bacteria.

RB: As a preliminary evaluation, it is crucial to investigate the effectiveness of pure photoactive RB against both *L. monocytogenes* and *S.* Typhimurium. For this purpose, the reduction in viable bacteria was determined by treating bacterial suspensions that contain different concentrations of

RB under white light irradiation for 40 min. RB at 20 ppm fully inhibited the growth of *L. monocytogenes* (Figure 5b) while it showed no activity against *S.* Typhimurium (Figure 5c), revealing a higher resistance of *S.* Typhimurium to RB. The weak bactericidal effect of RB on Gram-negative *E. coli* at high concentrations with light exposure was also observed by Li and coworkers.[32] The reason that Gram-negative bacteria were unaffected by RB could be related to the presence of an outer lipopolysaccharidic cell membrane, providing a physical and/or chemical barrier through which the singlet oxygen cannot penetrate and interact with the vital cellular targets (*e.g.,* membrane or cytoplasmic components). Previous studies reported that the minimum bactericidal concentration of RB was ~10 ppm.[33, 34] However, the minimum bactericidal concentration is greatly influenced by physicochemical characteristics of RB (*e.g.,* purity, solubility, etc.), types of the tested bacteria, and antibacterial testing protocols and conditions. It is worth mentioning that RB in the current study is hydrophilic and in the sodium form. In the absence of light, no antibacterial activity was detected for RB.

RB-ANCC: The reduction of bacterial cell counts at different concentrations of RB-ANCC is shown in Figures 6b and 6c. At the concentration of 25 ppm, RB-ANCC showed a 100% photo-bactericidal activity against *L. monocytogenes* (Figure 5b). While free RB had no antimicrobial effect on *S.* Typhimurium, RB-ANCC showed a significantly enhanced bactericidal effect at all tested concentrations (Figure 5c). This is likely due to the synergistic effect of cationic ANCC and photoactive RB in a conjugate form. Free primary amine groups of RB-ANCC might facilitate its adsorption onto the negatively charged bacterial cell wall, resulting in cell wall disruption and improved effectiveness of free radicals generated from RB by keeping RB in close proximity to bacteria. RB concentration of 100 ppm corresponding to ~630 ppm of RB-ANCC inhibited bacterial survival to ~80%. RB-ANCC conjugates also showed bactericidal activity without

exposure to light, and this is likely due to the existence of free amine groups on ANCC that induce cell disruption and lead cell death. In summary, a broader spectrum of antibacterial activity was achieved by linking RB onto ANCC to carry a high density of amine groups.

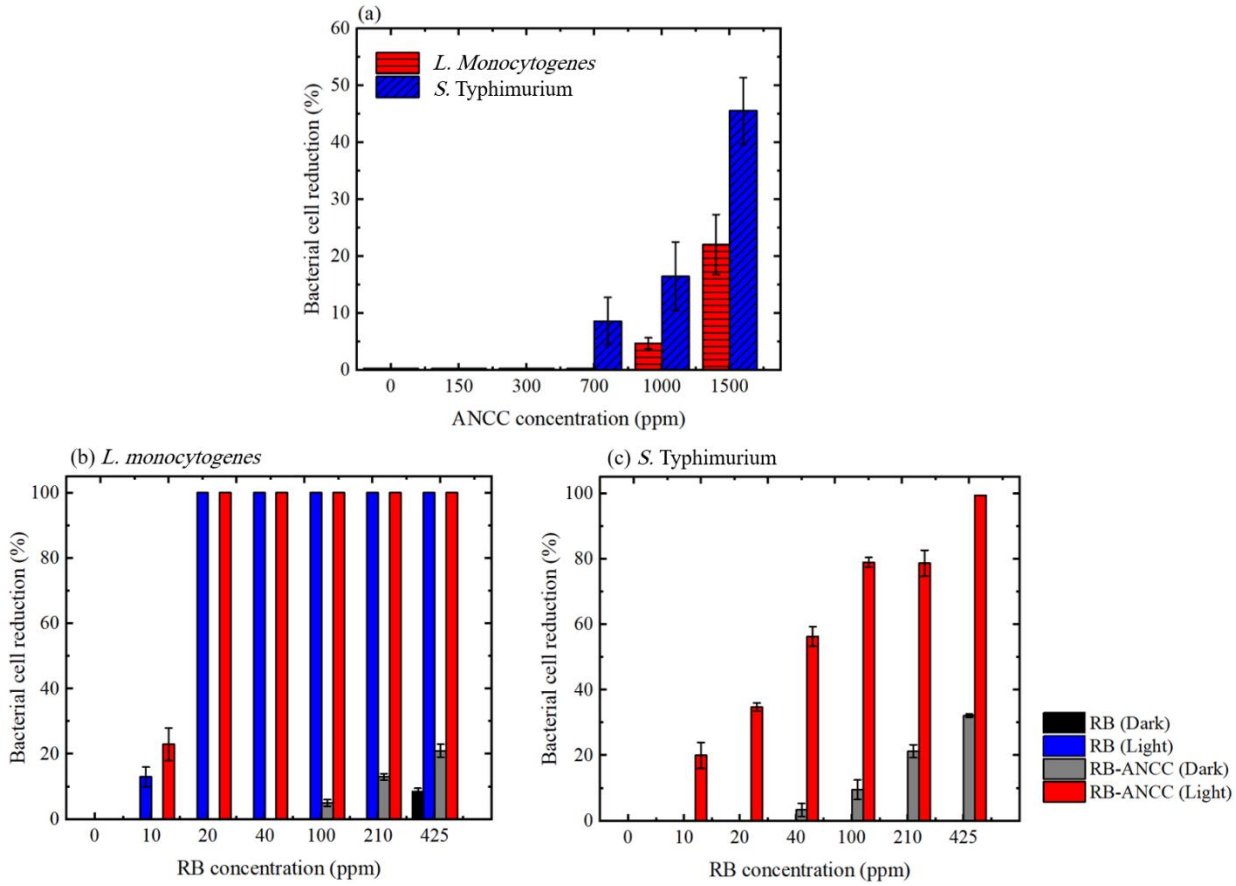

Figure 5. (a) Antimicrobial activity of ANCC against *L. monocytogenes* and *S.* Typhimurium after a 3-hrs contact; photo-bactericidal activity of free RB and RB-ANCC against (b) *L. monocytogenes* and (c) *S.* Typhimurium after 40 min light irradiation and dark condition. Horizontal axis refers to the concentration of grafted RB but not the concentration of RB-ANCC conjugate. The error bars represent the standard deviation of three independent replicates.

Bacterial Viability: CMF Films and CA Nanofibers

The antibacterial activity of CMF films and CA nanofibers against both foodborne pathogens was evaluated by using the plating assay (Figure 6a). Without the incorporation of RB-ANCC, CMF films and CA nanofibers showed no antimicrobial activity against *L. monocytogenes* and *S.*

Typhimurium. However, the remarkable antibacterial activity of films and nanofibers with RB-ANCC against both bacteria were observed once exposing them to light. Light-treated CMF films and CA nanofibers reduced the number of *L. monocytogenes* to ~100% (corresponding to a 6-log reduction) and ~80%, respectively. Besides, *S.* Typhimurium cell counts showed a decrease of ~70% for CMF film and ~60% for nanofibers when exposed to light. The difference in antibacterial properties of CMF films and CA nanofibers is due to different incorporation approaches of RB-ANCC. Specifically, photoactive RB-ANCC was electrostatically deposited onto the surface CMF films, but embedded in CA nanofibers. Therefore, the reduced ROS accessibility and/or electrostatic interaction in CA nanofibers would lower its photobactericidal efficiency. Overall, both films and nanofibers showed highly promising photobactericidal activity, but nanofibers are preferred for food packaging as photoactive nanofillers cannot leak out of the matrix (see Figure S7).

Disk Diffusion: CMF Film and CA Nanofiber

The disk diffusion assay was performed to assess the diffusibility of ROS and the antibacterial activity of photoactive CMF film and nanofibers incorporated with RB-ANCC. Films and nanofibers without RB-ANCC were used as the controls and exhibited no inhibitory effects, indicating that pure cellulosic films and nanofibers did not possess any antibacterial activity under both dark and light conditions. All the cellulosic materials incorporated with RB-ANCC displayed clear inhibition zones around the film discs after exposure to light (Figures 6b and 6c). However, CMF films containing electrostatically deposited RB-ANCC formed larger inhibition zones against both bacteria than those formed by CA nanofibers. These results were consistent with the results of bacterial cell reduction in contact with films (Figure 6a). The increased inhibition area formed around CMF film might result from the desorption of RB-ANCC conjugates, which may

diffuse to the agar during incubation with a high humidity. The reason for the detachment of cationic RB-ANCC nanofillers from anionic CMF films implemented on the plates could be explained by an exchange of RB-ANCC particles by charged nutrients/minerals of TSA media (*e.g.*, amino acids, peptides, sodium chloride). No bactericidal effect was observed in dark except for CMF films due to partial release of RB-ANCC (Figure 6a and 6b). The antibacterial activity of CMF films and CA nanofibers were also tested on the plates inoculated with bacterial suspension at the concentration of ~5 log CFU mL^{-1} and the pictures are available in the Supporting Information. As shown in Figure S8, the reduced inoculum resulted in an increasing trend of inhibition areas around nanofibers. Previous studies reported that photosensitizers could inactivate pathogens without direct contact by releasing singlet oxygen to the neighboring locations.[6, 35] It is also worth mentioning that extensive diffusibility of ROS to the neighboring locations is not required if the aim is to keep photobactericidal surface disinfected. In other words, the ability of the surfaces to inactivate pathogens via direct contact during light irradiation is more important.[36]

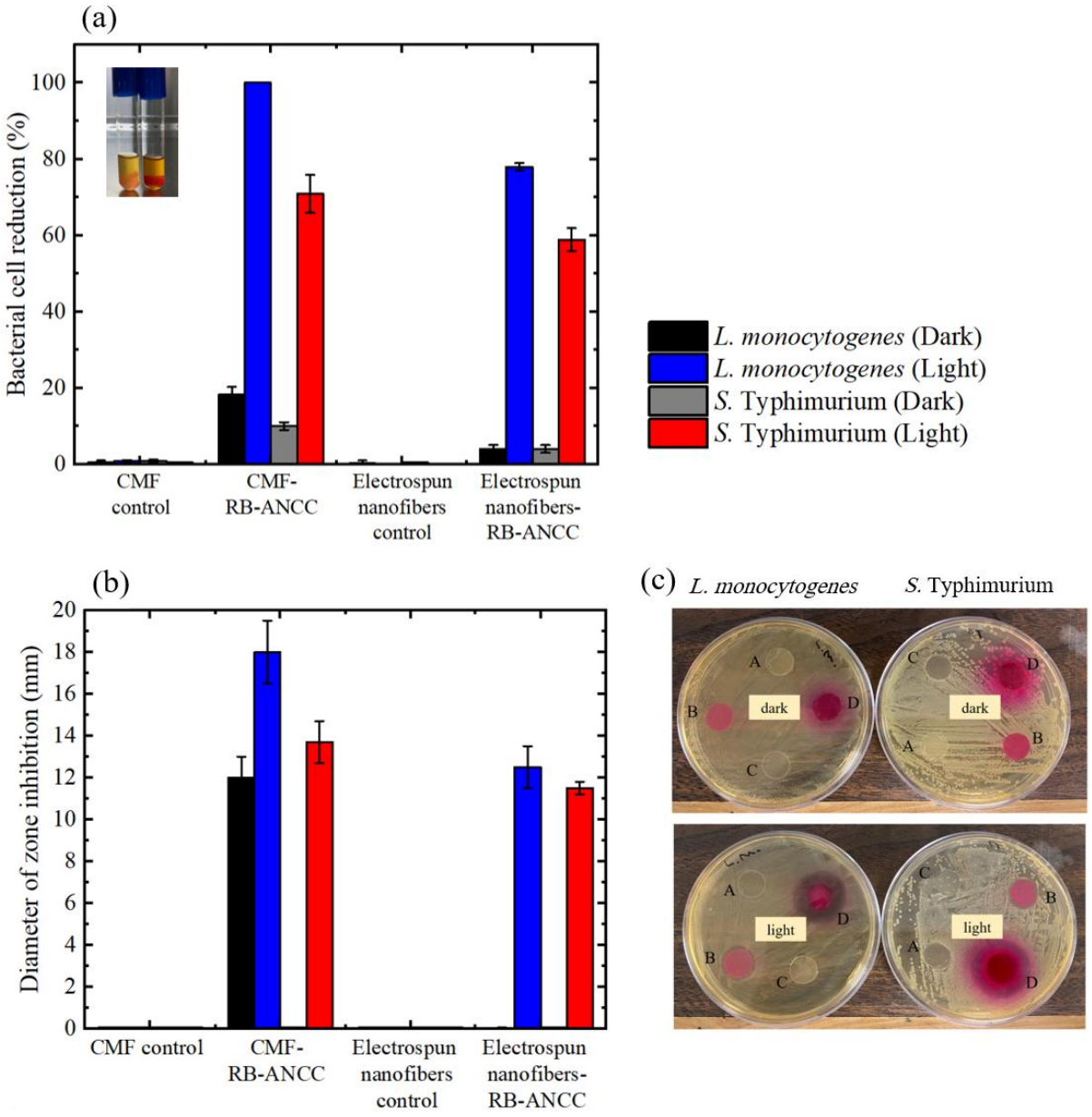

Figure 6. (a) Reduction of viable *L. monocytogenes* and *S.* Typhimurium cells treated with CMF film and CA nanofiber containing 2.5 wt. % RB-ANCC after 40 min light irradiation and dark condition; (b) zone of clearance of *L. monocytogenes* and *S.* Typhimurium bacterial lawns treated with CMF film and CA nanofiber containing 2.5 wt. % RB-ANCC after 40 min light irradiation and dark condition; (c) photobactericidal activities of electrospun CA nanofibers (A: control and B: with RB-ANCC) and CMF films (C: control and D: with RB-ANCC) evaluated by disk diffusion assay using 10^6 CFU mL^{-1} of bacteria. The dark zones around the central films/nanofibers imply the reduction of bacteria in those locations. The error bars in panels a and b represent the standard deviations of three independent replicates.

CONCLUSIONS

We have synthesized a photobactericidal HNC functionalized with photosensitizer RB. A DMTMM-mediated bioconjugation reaction was adopted for the covalent linking of carboxyl groups of RB to amine groups of HNC, without the need of any organic solvent. ANCC and RB both are naturally derived, biodegradable and biocompatible materials. The developed RB-ANCC conjugate showed promising antibacterial activity against Gram-positive and Gram-negative bacteria when exposed to normal white light. Two of the most abundant bacteria in foodborne diseases, *L. monocytogenes* and *S.* Typhimurium, were selected in this study for photo-bactericidal tests. We observed that RB has no bactericidal activity against *S.* Typhimurium, while RB-ANCC could kill ~80% at 100 ppm RB concentration. We also tested the RB-ANCC conjugate by combining it with two cellulose-based materials, by deposition on CMF films and by incorporation into mats of CA nanofibers, to see its efficiency in these materials. RB-ANCC CMF films could kill all 10^6 CFU mL^{-1} of *L. monocytogenes* bacteria and significantly reduce the *S.* Typhimurium population. This shows that attaching photosensitizers onto hairy ANCC increases its photo-bactericidal activity. In principle, a large number of photosensitizers can be loaded onto HNC which has a high density of reactive functional groups. Although RB was used here as a grafting agent on the bio-inspired ANCC, other natural photosensitizer molecules with carboxyl or aldehyde groups, *e.g.*, phloxine B or copper-chlorophilin, or a combination of different agents, can potentially be linked to ANCC to be used in the engineering photodynamically active cellulosic surfaces.

Supporting Information

Protocol of determining the aldehyde content; AFM and TEM imaging; standard calibration curve for RB determination (Figure S1); UV-vis absorption spectra of nanomaterials (Figure S2); preparation process of photodynamically active cellulosic surfaces (Figure S3); SEM images of electrospun nanofibers (Figure S4); bacteria-ANCC interaction (Figure S5); FTIR spectra of cellulose pulp, DAMC and ANCC (Figure S6); UV-vis absorption spectra of RB-ANCC desorbed from cellulosic surfaces (Figure S7); photographs of CMF films and CA nanofibers with RB-ANCC evaluated with the disk diffusion assay (Figure S8).

ACKNOWLEDGMENTS

The authors acknowledge financial support from the New Frontiers in Research Fund-Exploration (252808), Natural Sciences and Engineering Research Council Discovery Grants (250374), Natural Sciences and Engineering Research Council Discovery Launch Supplement (250531), and Natural Sciences and Engineering Research Council of Canada (NSERC-Discovery grant 2018-05781). Part of the user fees were covered by the FRQNT Quebec Centre for Advanced Materials. We also would like to thank Dr. Mohammad Hadi Moradian for providing CMF films.

REFERENCES

1. Food Safety https://www.who.int/news-room/fact-sheets/detail/food-safety. (accessed 30 April).
2. Song, B.; Zhang, E.; Han, X.; Zhu, H.; Shi, Y.; Cao, Z., Engineering and application perspectives on designing an antimicrobial surface. *ACS Applied Materials & Interfaces* **2020,** *12*, 21330-21341. DOI:10.1021/acsami.9b19992.
3. Silva, A. F.; Borges, A.; Giaouris, E.; Graton Mikcha, J. M.; Simões, M., Photodynamic inactivation as an emergent strategy against foodborne pathogenic bacteria in planktonic and sessile states. *Critical Reviews in Microbiology* **2018,** *44* (6), 667-684. DOI:10.1080/1040841X.2018.1491528.
4. Maldonado-Carmona, N.; Ouk, T.-S.; Calvete, M. J.; Pereira, M. M.; Villandier, N.; Leroy-Lhez, S., Conjugating biomaterials with photosensitizers: Advances and perspectives for photodynamic antimicrobial chemotherapy. *Photochemical & Photobiological Sciences* **2020,** *19* (4), 445-461. DOI:10.1039/C9PP00398C.
5. Hamblin, M. R.; Hasan, T., Photodynamic therapy: a new antimicrobial approach to infectious disease? *Photochemical & Photobiological Sciences* **2004,** *3* (5), 436-450. DOI: 10.1039/B311900A.
6. Stanley, S. L.; Scholle, F.; Zhu, J.; Lu, Y.; Zhang, X.; Situ, X.; Ghiladi, R. A., Photosensitizer-embedded polyacrylonitrile nanofibers as antimicrobial non-woven textile. *Nanomaterials* **2016,** *6* (4), 1-14. DOI:10.3390/nano6040077.
7. Rosely, C. S.; Joseph, A. M.; Leuteritz, A.; Gowd, E. B., Phytic Acid modified boron nitride nanosheets as sustainable multifunctional nanofillers for enhanced properties of poly (l-lactide). *ACS Sustainable Chemistry & Engineering* **2020,** *8* (4), 1868-1878. DOI:10.1021/acssuschemeng.9b06158.
8. Sahu, K.; Sharma, M.; Bansal, H.; Dube, A.; Gupta, P. K., Topical photodynamic treatment with poly-l-lysine–chlorin p6 conjugate improves wound healing by reducing hyperinflammatory response in Pseudomonas aeruginosa-infected wounds of mice. *Lasers in Medical Science* **2013,** *28* (2), 465-471. DOI:10.1007/s10103-012-1083-6.
9. Tegos, G. P.; Anbe, M.; Yang, C.; Demidova, T. N.; Satti, M.; Mroz, P.; Janjua, S.; Gad, F.; Hamblin, M. R., Protease-stable polycationic photosensitizer conjugates between polyethyleneimine and chlorin (e6) for broad-spectrum antimicrobial photoinactivation. *Antimicrobial Agents and Chemotherapy* **2006,** *50* (4), 1402-1410. DOI:10.1128/AAC.50.4.1402-1410.2006.
10. Simões, M.; Pereira, M. O.; Vieira, M. J., Action of a cationic surfactant on the activity and removal of bacterial biofilms formed under different flow regimes. *Water Research* **2005,** *39* (2-3), 478-486. DOI:10.1016/j.watres.2004.09.018.
11. Tan, Z.; Shi, Y.; Xing, B.; Hou, Y.; Cui, J.; Jia, S., The antimicrobial effects and mechanism of ε-poly-lysine against Staphylococcus aureus. *Bioresources and Bioprocessing* **2019,** *6* (1), 1-10. DOI:10.1186/s40643-019-0246-8.
12. Mahira, S.; Jain, A.; Khan, W.; Domb, A. J., Antimicrobial Materials—An Overview. In *Antimicrobial Materials for Biomedical Applications*, Royal Society of Chemistry: 2019.
13. Koshani, R.; van de Ven, T. G. M., Electroacoustic characterization of trimmed hairy nanocelluloses. *Journal of Colloid and Interface Science* **2020,** *563*, 252-260. DOI:10.1016/j.jcis.2019.12.034.

14. Moradian, M. H.; Islam, M. S.; van de Ven, T. G. M., Insoluble regenerated cellulose films made from mildly carboxylated dissolving and Kraft pulps. *Industrial & Engineering Chemistry Research* **2021,** *60*, 5385-5393. DOI:10.1021/acs.iecr.1c00485.
15. Yang, H.; Alam, M. N.; van de Ven, T. G. M., Highly charged nanocrystalline cellulose and dicarboxylated cellulose from periodate and chlorite oxidized cellulose fibers. *Cellulose* **2013,** *20* (4), 1865-1875. DOI:10.1007/s10570-013-9966-7.
16. Koshani, R.; van de Ven, T. G. M., Carboxylated cellulose nanocrystals developed by Cu-assisted H_2O_2 oxidation as green nanocarriers for efficient lysozyme immobilization. *Journal of Agricultural and Food Chemistry* **2020,** *68* (21), 5938-5950. DOI:10.1021/acs.jafc.0c00538.
17. Hosseinidoust, Z.; Alam, M. N.; Sim, G.; Tufenkji, N.; van de Ven, T. G. M., Cellulose nanocrystals with tunable surface charge for nanomedicine. *Nanoscale* **2015,** *7* (40), 16647-16657. DOI:10.1039/C5NR02506K.
18. Koshani, R.; Tavakolian, M.; van de Ven, T. G. M., Natural emulgel from dialdehyde cellulose for lipophilic drug delivery. *ACS Sustainable Chemistry & Engineering* **2021,** *9*, 4487−4497. DOI:10.1021/acssuschemeng.0c08692.
19. Jiao, W.; Wu, Y.; Lu, G.; Jing, H., Inhibition of the excited-state Rose Bengal (RB) nonradiative process by introducing DMSO for highly efficient photocatalytic hydrogen evolution. *RSC Advances* **2016,** *6* (35), 29538-29544. DOI:10.1039/C6RA01998F
20. Heidari Nia, M.; Tavakolian, M.; Kiasat, A. R.; van de Ven, T. G. M., Hybrid aerogel nanocomposite of dendritic colloidal silica and hairy nanocellulose: an effective dye adsorbent. *Langmuir* **2020,** *36* (40), 11963-11974. DOI:10.1021/acs.langmuir.0c02090.
21. Estevao, B. M.; Cucinotta, F.; Hioka, N.; Cossi, M.; Argeri, M.; Paul, G.; Marchese, L.; Gianotti, E., Rose Bengal incorporated in mesostructured silica nanoparticles: structural characterization, theoretical modeling and singlet oxygen delivery. *Physical Chemistry Chemical Physics* **2015,** *17* (40), 26804-26812. DOI:10.1039/C5CP03564C
22. Koshani, R.; van de Ven, T. G. M.; Madadlou, A., Characterization of carboxylated cellulose nanocrytals isolated through catalyst-assisted H2O2 oxidation in a one-step procedure. *Journal of Agricultural and Food Chemistry* **2018,** *66* (29), 7692-7700. DOI:10.1021/acs.jafc.8b00080.
23. Newman, R. H., Estimation of the lateral dimensions of cellulose crystallites using 13C NMR signal strengths. *Solid State Nuclear Magnetic Resonance* **1999,** *15* (1), 21-29. DOI:10.1016/S0926-2040(99)00043-0.
24. Heidari Nia, M., Koshani, R., Munguia-Lopez, J. G., Kiasat, A. R., Kinsella, J. M., van de Ven, T. G. M., Biotemplated hollow meso-porous silica particles as efficient carriers for drug delivery. *ACS Applied Bio Materials* **2021,** *4*, 4201-4214. DOI:10.1021/acsabm.0c01671.
25. Wang, Y.; Chen, L., Cellulose nanowhiskers and fiber alignment greatly improve mechanical properties of electrospun prolamin protein fibers. *ACS applied materials & interfaces* **2014,** *6* (3), 1709-1718.
26. Luksiene, Z.; Buchovec, I.; Paskeviciute, E., Inactivation of several strains of Listeria monocytogenes attached to the surface of packaging material by Na-chlorophyllin-based photosensitization. *Journal of Photochemistry and Photobiology B: Biology* **2010,** *101* (3), 326-331. DOI:10.1016/j.jphotobiol.2010.08.002.
27. Baron, S., Salmonella. In *Medical Microbiology*, 4th ed.; University of Texas Medical Branch at Galveston: 1996.

28. Fei Liu, X.; Lin Guan, Y.; Zhi Yang, D.; Li, Z.; De Yao, K., Antibacterial action of chitosan and carboxymethylated chitosan. *Journal of Applied Polymer Science* **2001,** *79* (7), 1324-1335. DOI:0.1002/1097-4628(20010214)79:7<1324::AID-APP210>3.0.CO;2-L.
29. Gilbert, P.; Al‐taae, A., Antimicrobial activity of some alkyltrimethylammonium bromides. *Letters in Applied Microbiology* **1985,** *1* (6), 101-104. DOI:10.1111/j.1472-765X.1985.tb01498.x.
30. Marinelli, L.; Di Stefano, A.; Cacciatore, I., Carvacrol and its derivatives as antibacterial agents. *Phytochemistry Reviews* **2018,** *17* (4), 903-921. DOI:10.1007/s11101-018-9569-x.
31. Petushkov, A.; Intra, J.; Graham, J. B.; Larsen, S. C.; Salem, A. K., Effect of crystal size and surface functionalization on the cytotoxicity of silicalite-1 nanoparticles. *Chemical Research in Toxicology* **2009,** *22* (7), 1359-1368. DOI:10.1021/tx900153k.
32. Li, C.; Lin, F.; Sun, W.; Wu, F.-G.; Yang, H.; Lv, R.; Zhu, Y.-X.; Jia, H.-R.; Wang, C.; Gao, G., Self-Assembled rose bengal-exopolysaccharide nanoparticles for improved photodynamic inactivation of bacteria by enhancing singlet oxygen generation directly in the solution. *ACS Applied Materials & Interfaces* **2018,** *10* (19), 16715-16722. DOI:10.1021/acsami.8b01545.
33. Chan, B.; Chan, O.; So, K.-F., Effects of photochemical crosslinking on the microstructure of collagen and a feasibility study on controlled protein release. *Acta Biomaterialia* **2008,** *4* (6), 1627-1636. DOI:10.1016/j.actbio.2008.06.007.
34. Shrestha, A.; Kishen, A., Polycationic chitosan‐conjugated photosensitizer for antibacterial photodynamic therapy. *Photochemistry and Photobiology* **2012,** *88* (3), 577-583. DOI:10.1111/j.1751-1097.2011.01026.x.
35. Dahl, T.; RobertMiddenand, W.; Hartman, P., Pure singlet oxygen cytotoxicity for bacteria. *Photochemistry and Photobiology* **1987,** *46* (3), 345-352. DOI:10.1111/j.1751-1097.1987.tb04779.x.
36. Querido, M. M.; Aguiar, L.; Neves, P.; Pereira, C. C.; Teixeira, J. P., Self-disinfecting surfaces and infection control. *Colloids and Surfaces B: Biointerfaces* **2019,** *178*, 8-21. DOI:10.1016/j.colsurfb.2019.02.009.

For Table of Contents Use Only.

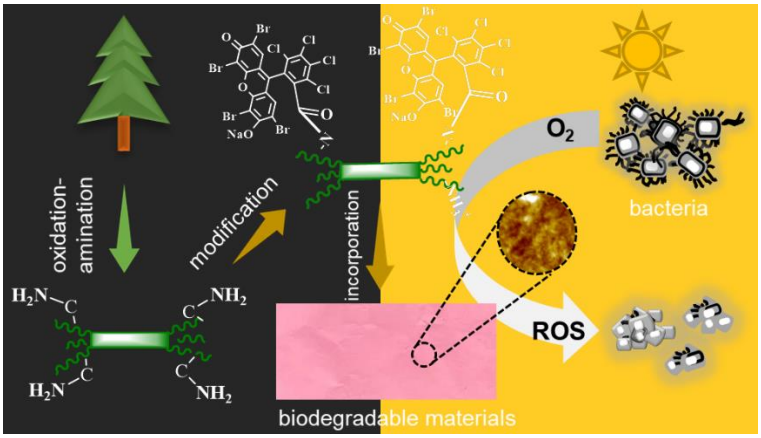

Synopsis

A sustainable photobactericidal nanofiller was rationally engineered from aminated hairy nanocrystalline cellulose functionalized with natural photoactive rose-bengal through bioconjugation.